Low-temperature phase transitions in barium sodium niobate

2007 J. Phys.: Condens. Matter 19 236206

(http://iopscience.iop.org/0953-8984/19/23/236206)

IOP PUBLISHING JOURNAL OF PHYSICS: CONDENSED MATTER

J. Phys.: Condens. Matter **19** (2007) 236206 (14pp) doi:10.1088/0953-8984/19/23/236206

Low-temperature phase transitions in barium sodium niobate

C Filipic[1], Z Kutnjak[1], R Lortz[2], A Torres-Pardo[2,4], M Dawber[2] and J F Scott[3]

[1] Jozef Stefan Institute, Ljubljana, SI-60001, Slovenia
[2] DPMC, University of Geneva, 24 quai Ernest-Ansermet, 1211 Geneva 4, Switzerland
[3] Earth Sciences Department, Cambridge University, Cambridge CB2 3EQ, UK

E-mail: matthew.dawber@physics.unige.ch

Received 14 March 2007, in final form 16 April 2007
Published 8 May 2007
Online at stacks.iop.org/JPhysCM/19/236206

Abstract

We present dielectric and specific heat data on barium sodium niobate ($Ba_2Na_{1-x}Nb_5O_{15}$) from 4 to 460 K with an emphasis on the low-temperature incommensurate phase transitions. This material is ferroelectric below $T_c(x) =$ ca 830 K, and the reciprocal dielectric constant extrapolates to zero near this temperature throughout the low-temperature phases, which involve distortions within the non-polar plane and do not affect significantly the ferroelectric properties. The transition from orthorhombic to incommensurate near 113 K has highly frequency-dispersive dynamics, reminiscent of those in relaxors, and an activation energy of 0.42 eV. The 'lock-in' transition near 30 K to a tetragonal structure with an enlarged unit cell has been controversial, with studies in Japan (1996, 1997) and the Czech Republic (2004) not finding the $P4nc$ phase predicted by Schneck (1982) and measured directly via spallation neutron scattering by Scott *et al* (1990); our new studies show that this transition is limited by kinetics and requires very slow cooling for detection.

(Some figures in this article are in colour only in the electronic version)

1. Introduction

Barium sodium niobate is a tungsten bronze structure that is ferroelectric with six phase transitions at ambient pressure and three incommensurate phases. Unlike most incommensurate insulators, it remains ferroelectric throughout its incommensurate phases, with polarization P normal to the direction(s) of modulation. At least two of the incommensurate phases vanish above a hydrostatic pressure of $p = 5$ kbar. A recent study [1] characterized the four

[4] Permanent address: Dipartemento de Química Inorgánica, Facultad de Químicas, Universidad Complutense, Madrid-28040, Spain.

phase transitions above ambient temperature with an emphasis on the critical exponents for thermodynamic quantities near its ferroelectric phase transition temperature (of about 830 K), which are those of a mean-field transition near a tricritical point. The transition is of special theoretical interest because the order parameter is four-dimensional, which is unusual but not unique (cf $BaMnF_4$). A further complication of interest is the fact that $T_c(x)$ varies significantly with Na–vacancy concentration x in this material, from about 810–850 K. A second recent review [2] focused attention on the low-temperature transitions, and in particular the presence or absence of a low-temperature lock-in transition for the incommensurate phase below 100 K, as well as on a previously unreported doubling of the primitive cell along the b-axis. Such incommensurate phases are generally known to be stabilized by defects and vacancies, so the absence of such a lock-in transition in some specimens [3, 4] would not be surprising. This situation would actually be of considerable interest because, as shown recently by Cano and Levanyuk [5], an incommensurate phase persisting to $T = 0$ should exhibit a specific heat linear in T, unlike most insulators. The lock-in phase had been predicted by Schneck [6] to have tetragonal $P4nc$ space group symmetry with a unit cell enlarged from that of the ambient orthorhombic phase, and this was confirmed by Scott *et al* [7] in one sample. However, the incommensurate phase can be stabilized by defects, including Na–vacancies, so in the present work we examine two specimens with Na–vacancy concentrations known to be very different (about 0.5% and 3%). We note that transitions which increase in point group symmetry with lowering temperature (in this case from orthorhombic to tetragonal) are uncommon but thermodynamically and symmetry allowed, particularly if they increase the size of the primitive unit cell.

2. The incommensurate transition near 100 K

2.1. Prior work

Following its original discovery by Schneck *et al* [8], the most recent studies of the low-temperature phase transition near 100 K are by Mori *et al* [3] and Fujishiro and Uesu [4] and are reviewed by Buixaderas *et al* [2]. Reference [3] shows a transmission electron microscopy (TEM) study down to 25 K which finds that the quasi-commensurate $Ccm2_1$ phase becomes a $2q$ quasi-tetragonal phase below a broad phase transition that actually begins around 200 K and extends down to 100 K. Mori *et al* claim that their diffraction patterns show that the low-temperature phase has a unit cell $4\times$ that of the room-temperature phase, with $2a \times 2b \times c$ of that orthorhombic phase, in agreement with earlier studies at 105 K by Verweft *et al* [9, 10], who concluded that this material is tetragonal below 110 K, and with Schneck *et al* [11, 12], who showed that this depends upon samples and their individual Na–vacancy concentration. However, the diffraction patterns in the work of Mori *et al* also reveal extra diffraction maxima located at $(0\ k/2\ l/2)$ and diffuse maxima at $(h/2\ k\ l/2)$, which require a $2a \times 2b \times 2c$ unit cell; hence this lattice periodicity is actually $8\times$ that of the room-temperature phase.

Oliver and Scott [13] showed that the hysteresis behaviour in the dielectric constant (cooling versus heating) was present from about 40 to 110 K, thus limiting the inferred incommensurate $2q$ phase to that temperature range. (More recent evidence puts the upper transition closer to 113 K and the lower transition closer to 30 K.) They also found at 10 K that the spallation neutron scattering diffraction spots could be indexed to a $P4nc$ tetragonal lock-in phase. In general, the various results show that sample variability, and in particular their Na–vacancy concentration, determines whether there is a lock-in transition or if the incommensurate structure persists to extremely low temperatures, with antiphase boundaries pinned and stabilized by vacancies.

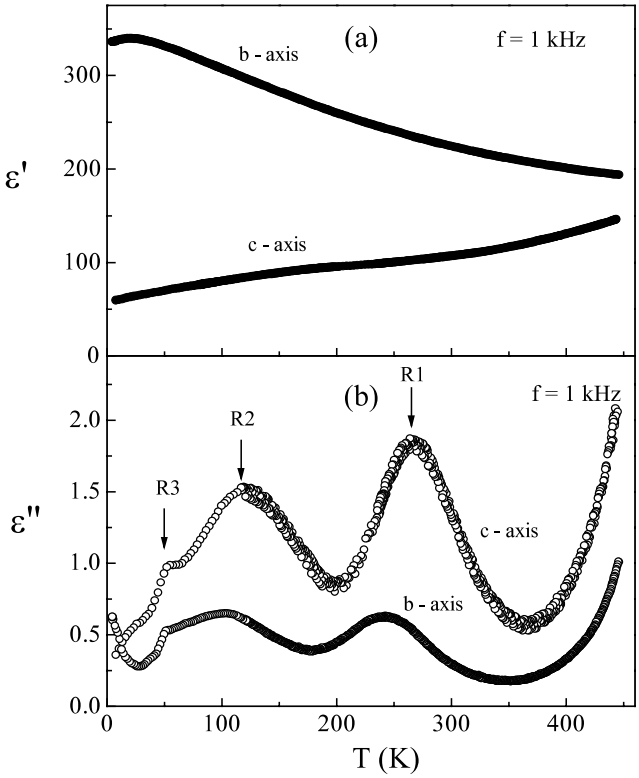

Figure 1. Temperature dependence of the dielectric constant ε' (a) and ε'' (b) obtained in BNN along *b*- and *c*-axes at a frequency of 1 kHz.

2.2. New dielectric studies

We have analysed two specimens of barium sodium niobate ($Ba_2NaNb_5O_{15}$), abbreviated as BNN, having different Na–vacancy concentrations (established from earlier work [1]). Dielectric data were run for all axes of both samples, but no significant differences were observed for the two samples in the present work. Although there is a small shift between the absolute values of the dielectric constants, only near the ferroelectric transition at about 835 K (studied in [1]) are effects from the Na–vacancy concentration significant. The two samples had different shapes, making electroding of the *c*-face easier (and the data better) for one, and of the *b*-face for the other. The better quality data for each axis are shown in the following figures.

The real (ε') and the imaginary (ε'') parts of the complex dielectric constant were measured as a function of the temperature and frequency (1 mHz–1 MHz) using a Novocontrol Alpha Analyzer. The temperature of the samples was stabilized by an Oxford instruments continuous-flow cryostat and ITC4 temperature controller in the temperature range between 4.2 and 460 K.

Both specimens exhibit several anomalies in the real ε' and imaginary ε'' parts of the complex dielectric constant in the studied temperature interval between 4.2 and 460 K (figure 1). Figure 1(a) shows the temperature dependence of the real part of the dielectric constant, measured at 1 kHz, along the *b*- and *c*-axes.

From figure 1(a) it is obvious that both temperature dependences are qualitatively different. While the values of the dielectric constant measured along the *b*-axis decrease with increasing temperature, the values measured along the *c*-axis increase. The increase in the dielectric constant observed along the *c*-axis is related to the ferroelectric phase transition at high

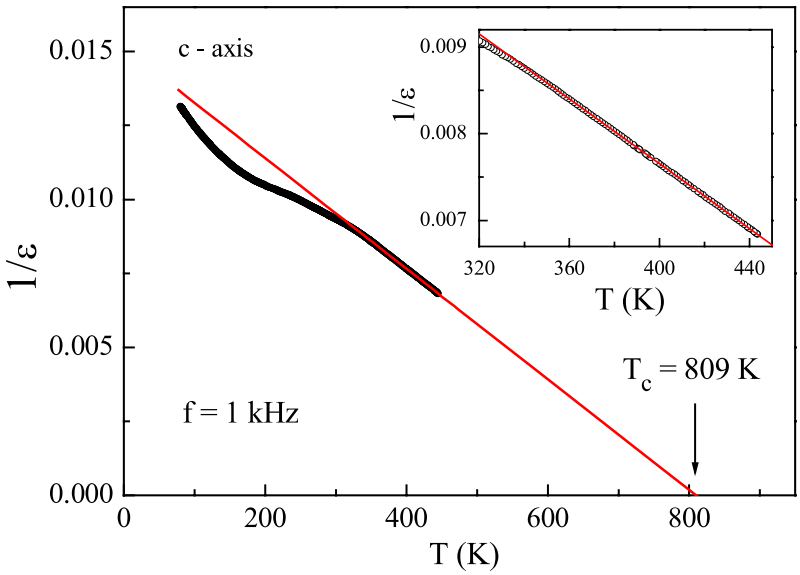

Figure 2. Temperature dependence of the inverse dielectric constant ($1/\varepsilon'(T)$), measured along the c-axis in BNN at 1 kHz. Extrapolation over a very wide range of temperatures (>100 K) gives $T_c = 809$ K (inset).

temperatures. In fact $1/\varepsilon'(T)$, measured along the c-axis, follows the Curie–Weiss law (figure 2), thus signalling the onset of the phase transition at high temperature. An extrapolation over a very wide range of temperatures (>100 K) gives a transition temperature of 809 K, which agree reasonably with the known Curie temperature $T \approx 840$ K (see [1] and references therein).

Figure 1(b) shows the temperature dependence of the imaginary part of the dielectric constant, measured at 1 kHz, along the b- and c-axes. In contrast to the behaviour observed in the real part of the dielectric constant, figure 1(b) shows similar temperature dependences of ε'' in the whole temperature range studied for both the b and c directions, except for the slightly higher ε'' values, measured along the c-axis.

If we look at two temperature dependences of the imaginary dielectric constant, three distinctive anomalies can easily be identified (denoted by arrows in figure 1(b)). After the analysis of the frequency scans at different temperatures, we conclude that the observed maxima in ε'' (denoted in figure 1(b) by R1, R2, and R3) are not static phenomena, but are of purely dynamic origin being related to the existence of the three distinctive dielectric relaxations. Same denotations of dielectric relaxations are valid for both axes, since the same dynamic response is expected in both axes. Due to different Na–vacancy concentrations of the samples, the characteristic relaxation frequencies of one axis were found to be slightly shifted against those determined in the other axis.

The complex dielectric constant data for the c-axis are shown in figure 3 in an Argand plot, where ε'' is plotted versus ε' at three different temperatures. At higher temperatures (305 K) only one semicircle with a centre below the ε' axis is seen in the frequency window of our experiment. We denote this relaxation by R1. By lowering the temperature to 205 K, a second relaxation appears in our frequency window, in addition to the first one. We denoted it by R2. This relaxation exhibits much higher characteristic frequency and dielectric relaxation strength than R1. By lowering the temperature the characteristic frequencies of relaxation, R1 and R2, decrease significantly, consequently the relaxation R1 escapes the experimental frequency window below approximately 150 K.

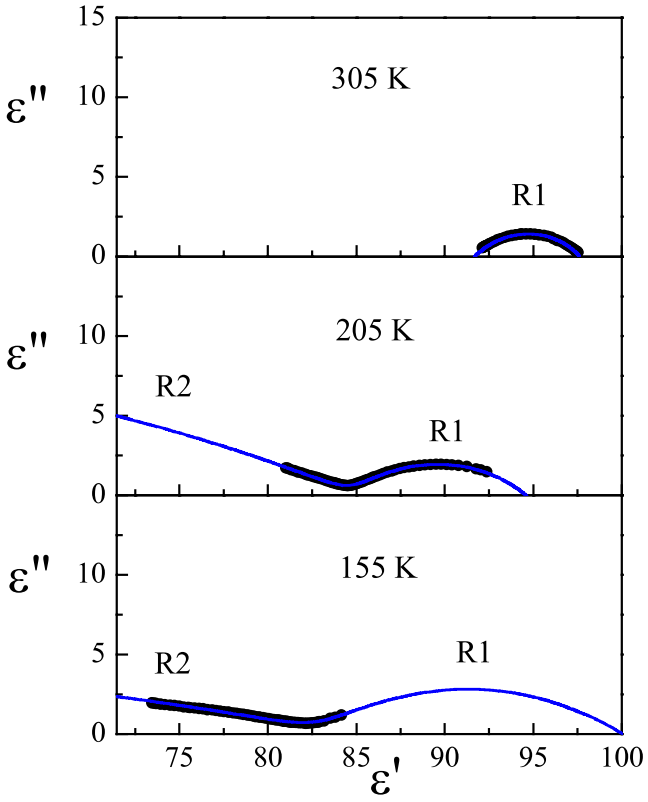

Figure 3. ε'' plotted versus ε' at three different temperatures in the BNN c-axis sample. Solid lines are fits with the Cole–Cole expression (equation (1)). Labels R1 and R2 denote the first and second relaxations.

Experimental data of both relaxations are fitted with the Cole–Cole expression

$$\varepsilon^* = \varepsilon_{\infty 2} + \frac{\Delta\varepsilon_2}{1 + (\mathrm{i}\omega\tau_2)^{1-h_2}} + \frac{\Delta\varepsilon_1}{1 + (\mathrm{i}\omega\tau_1)^{1-h_1}}, \tag{1}$$

where subscripts 1 and 2 denote the first (R1) or the second (R2) relaxations, respectively.

Here the dielectric relaxation strength $\Delta\varepsilon_i = \varepsilon_{0i} - \varepsilon_{\infty i}$, the characteristic relaxation time τ_i, and the parameter describing the distribution of the relaxation times h_i play a role of fitting parameters. If $h = 0$, the relaxation is monodispersive, while for $0 < h < 1$ the relaxation is polydispersive; i.e. there is a distribution of relaxation times in the system. ε_{0i} is the static dielectric constant, and $\varepsilon_{\infty i}$ is the dielectric constant at high frequencies.

Figure 4 shows the temperature dependence of the characteristic relaxation frequency $f_1 = 1/(2\pi\tau_1)$ of the first relaxation (R1) obtained by fitting data, at each temperature, with equation (1). The temperature dependence of the relaxation frequency f_1 follows the Arrhenius law $f_1 = f_{01}\exp(-\Delta U_1/T)$. Values of the fit parameters obtained by fitting the data in figure 4 (solid lines in figure 4) are $f_{01} = 1.3 \times 10^{11}$ Hz and $\Delta U_1 = 0.42$ eV. There are several possible sources of this energy, but kink diffusion is most likely. From nuclear magnetic resonance (NMR), Munteau and Ailion found 0.47 ± 0.05 eV in $Ba_2NaNb_5O_{15}$ (the present material), and they interpreted that as an activation energy for the slow diffusion of incommensurate kinks, which they found to persist from 15 to 540 K [14].

Figure 4 also shows the temperature dependence of f_1 determined for the b-axis. As mentioned before, the characteristic frequencies are slightly shifted in temperature due to different Na–vacancy concentrations of the samples.

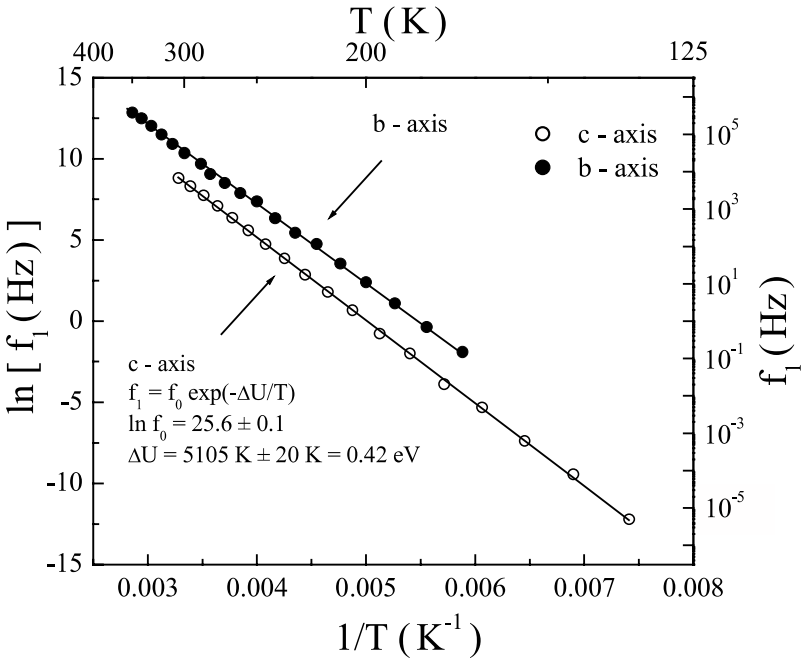

Figure 4. Temperature dependence of the characteristic relaxation frequency f_1 obtained in the *b*- and *c*-axes of BNN. Solid lines are fits to the Arrhenius law.

Figure 5 shows the temperature dependence of the static dielectric constant, ε_{01}, and the dielectric constant at high frequencies, $\varepsilon_{\infty 1}$, of the R1 relaxation measured along the *c*-axis. Both parameters were determined by fitting the dielectric data at each temperature with equation (1). Below 150 K the characteristic frequency f_1 decreases so much that most of the R1 relaxation leaves the experimental frequency window, which precludes the determination of ε_{01} at lower temperatures. Both values ε_{01} and $\varepsilon_{\infty 1}$ at higher temperatures decrease with decreasing temperature. At lower temperatures ($T < 200$ K), $\varepsilon_{\infty 1}$ saturates to an approximately constant value of about 85, but the ε_{01} starts to increase again below 230 K.

Figure 6 shows the temperature dependence of the dielectric strength $\Delta\varepsilon_1 = \varepsilon_{01} - \varepsilon_{\infty 1}$ of the R1 relaxation, measured along the *c*-axis. The dielectric strength increases with decreasing temperature and reaches a value of about 20 at 150 K. Since the dielectric strength of the R1 relaxation decreases with increasing temperature, which means that this relaxation cannot be interpreted as a soft mode related to the ferroelectric transition at $T_c \approx 840$ K.

The polydispersivity of the R1 relaxation does not change in the studied temperature region, with h_1 being approximately 0.6. In contrast to this, the second relaxation becomes more polydispersive by lowering the temperature. The h_2 increases from 0.2 at high temperatures to 0.8 at 150 K. It is necessary to mention that $\varepsilon_{\infty 2}$, the dielectric constant at high frequencies of the second relaxation R2, which enters the frequency window of the experiment below 210 K, could not be determined directly from the experiment due to the very high relaxation frequency of this relaxation. Therefore the best-fit value of $\varepsilon_{\infty 2} = 30$ was fixed at all temperatures. The dielectric strength of the second relaxation was determined by $\Delta\varepsilon_2 = \varepsilon_{01} - 30$. Namely, the static dielectric constant of the second relaxation is $\varepsilon_{02} = \varepsilon_{\infty 1}$. Since ε_{02} increases with increasing temperature, this relaxation can be identified as a main contribution to the total dielectric constant increase with increasing temperature toward $T_c \approx 840$ K (see figures 1(a) and 2), possibly linking this relaxation to the ferroelectric soft mode.

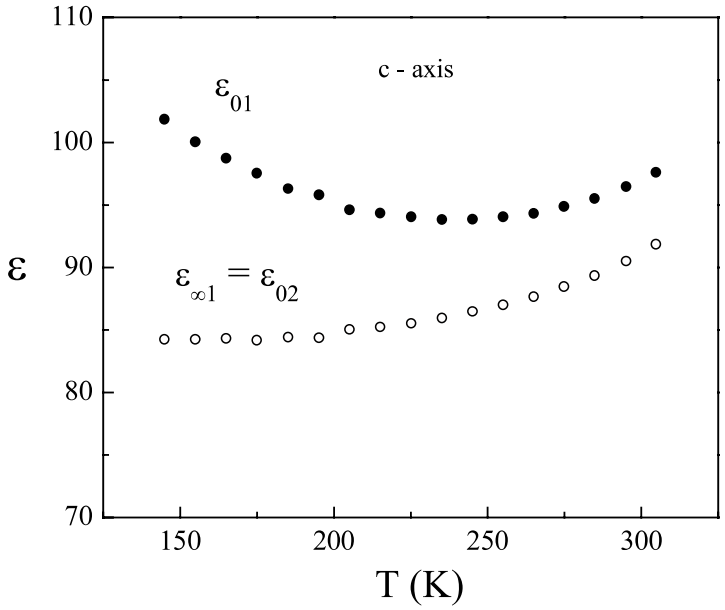

Figure 5. Temperature dependence of the static dielectric constant, ε_{01}, and the dielectric constant at high frequencies, $\varepsilon_{\infty 1}$, of the R1 relaxation measured along the *c*-axis of BNN. Both values were determined by fitting the frequency-dependent dielectric data at a given temperature with equation (1).

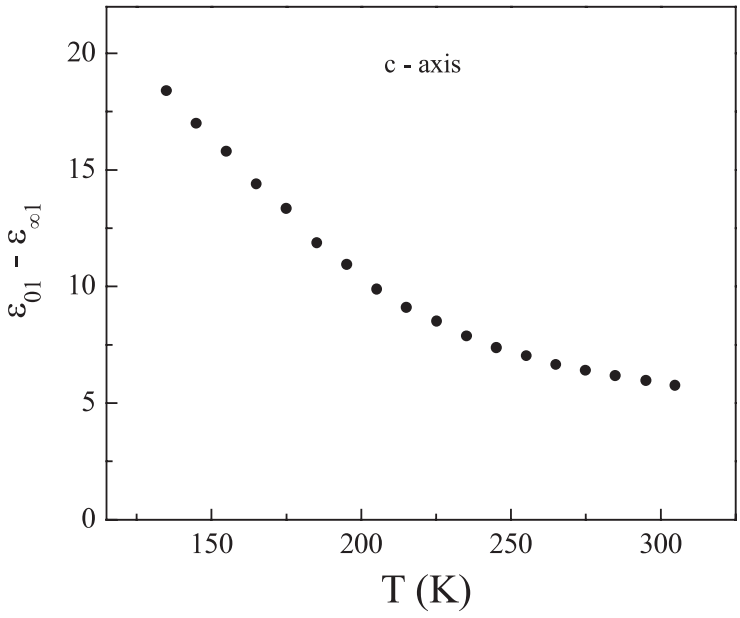

Figure 6. Temperature dependence of the dielectric strength $\Delta\varepsilon_1 = \varepsilon_{01} - \varepsilon_{\infty 1}$ of R1 relaxation, measured along the *c*-axis of BNN.

As indicated by figure 3, the second relaxation R2 becomes progressively suppressed with decreasing temperature, i.e. the system becomes more polydispersive at lower temperatures.

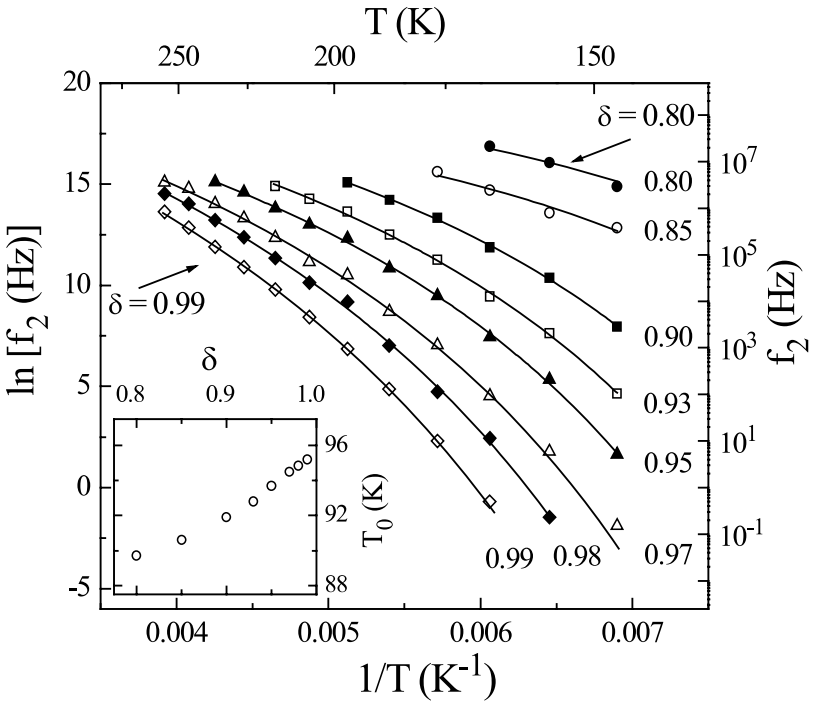

Figure 7. Temperature–frequency plot for several values of reduced dielectric constant δ (top to bottom: 0.80, 0.85, 0.90, 0.93, 0.95, 0.97, 0.98, and 0.99) in BNN along the *c*-axis. Solid lines are fits obtained with a generic Vogel–Fulcher expression. The inset shows the dependence of the Vogel–Fulcher temperature T_0 on δ.

In order to extract information on the temperature variation of the relaxation spectrum of the second relaxation and thus on the dynamic process, we analysed the R2 dielectric dispersion in BNN using the temperature–frequency plot applied recently to various glassy and relaxor systems [16–18]. An extensive description of this method was already given elsewhere [15, 17]. Here an assumption is adopted that the distribution of relaxation times, $g(z)$, is limited by the lower and upper cutoffs z_1 and z_2, respectively, where $z_i = \ln(\omega_a \tau_i)$ with ω_a as an arbitrary unit frequency. By varying the reduced dielectric constant δ

$$\delta = \frac{\varepsilon'(\omega, \tau) - \varepsilon_\infty}{\varepsilon_0 - \varepsilon_\infty} = \int_{z_1}^{z_2} \frac{g(z)\,\mathrm{d}z}{1 + (\omega/\omega_a)^2 \exp(2z)}, \tag{2}$$

between the values 1 and 0, the filter in the second part of equation (2) probes the distribution of relaxation times $g(z)$ by shifting its position in ω space [16] (at $\delta = 1$ the upper limit of the relaxation spectrum is probed, i.e. the longest relaxation time).

Characteristic temperature–frequency plots for each fixed value of the reduced dielectric constant δ between 0.80 and 0.99 are shown in figure 7. It is clearly seen that different parts of the relaxation spectrum diverge at different freezing temperatures. All the data for $\delta > 0.8$ above 150 K can be effectively described by a Vogel–Fulcher law ($f_2 = f_{02} \exp[-\Delta U_2/(T - T_0)]$). The parameters f_{02}, ΔU_2, and T_0 were determined by fitting each curve in figure 7 with the Vogel–Fulcher expression. The inset shows the dependence of the Vogel–Fulcher temperature T_0 on δ. The freezing temperature, where the longest relaxation diverges, was determined as $T_f = T_0(\delta \to 1) = 95.7 \pm 0.3$ K. Similar behaviour due to the freezing of the domain wall motions was found in KD_2AsO_4 and KH_2AsO_4 [19–21].

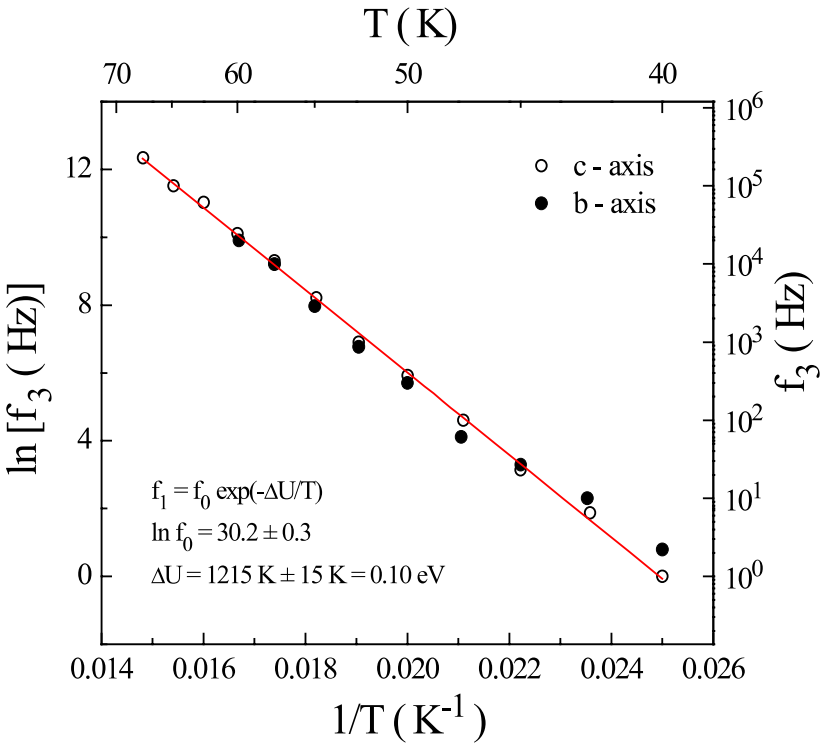

Figure 8. Temperature dependence of the relaxation frequency f_3 of the R3 relaxation, measured along the *b*- and *c*-axes of BNN.

Below 70 K the third relaxation (R3) enters the frequency window of the experiment. This relaxation exhibits relatively small dielectric strength ($\Delta\varepsilon_3 = \varepsilon_{03} - \varepsilon_{\infty 3} \approx 0.5$), but still it was possible to determine the temperature dependence of the characteristic frequency. Figure 8 shows the temperature dependence of the relaxation frequency of the R3 relaxation f_3, measured in both axes. The temperature dependence of the relaxation frequency f_3 follows the Arrhenius law $f_3 = f_{03} \exp(-\Delta U_3/T)$ in the temperature interval between 40 and 70 K. Parameters of the fit are $f_{03} = 1.3 \times 10^{13}$ Hz and $\Delta U_3 = 0.10$ eV. The physical origin of this third relaxation is unknown, but [22] shows that a value of about 0.1 eV is characteristic of many tetragonal tungsten bronze relaxors at cryogenic temperatures.

It is rather remarkable in that there are three intervening phase transitions; however, this occurs because the ferroelectric polarization P_z is orthogonal to the planar distortions in the xy-plane at those transition temperatures.

3. The lock-in transition near 30 K

3.1. Prior controversy

Earlier work, as described in section 2 above, suggests that the existence of a lock-in phase transition to a commensurate structure at $T \ll 110$ K may be sample dependent. In addition, there is a good possibility that the phase transition near 40 K—evident in both dielectric [13] and neutron scattering studies [7]—is primarily a distortion of oxygen ion positions. The neutron scattering data have the advantage that they are very sensitive to the position of the oxygen

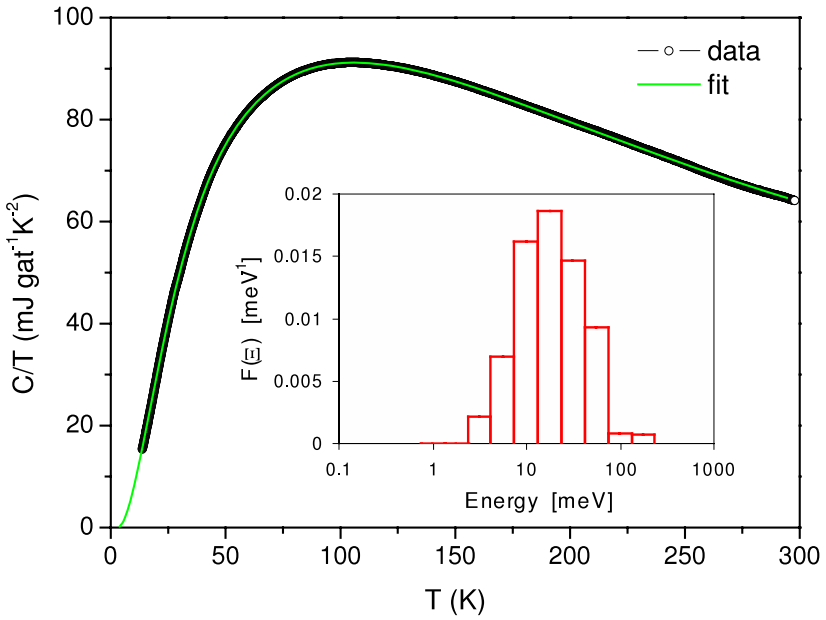

Figure 9. Specific heat divided by absolute temperature $C(T)/T$ for barium sodium niobate from 15–300 K. The fit assumes eight Einstein modes for phonons, shown as a bar graph in the insert.

ions, whereas x-ray or electron microscopy generally gives accurate information for only the heavy Ba or Nb ions in this material. Thus it is not surprising that x-ray and SEM/TEM reveal no phase transition near 40 K, whereas neutron scattering does, since most phase transitions in tungsten bronze oxides involve oxygen displacements rather than heavy-ion movement.

3.2. Low temperature specific heat data

The specific heat was measured with a continuous heating adiabatic calorimeter on a 80 mg sample (the sample with the lower Na vacancy concentration) between 15 and 300 K and on a smaller ∼20 mg sample (the sample with the higher Na vacancy concentration) with a high-resolution ac heat-flow calorimeter between 10 and 60 K. Figure 9 shows the total specific heat in the full temperature range. The inset of this figure illustrates a bar graph of phonon features, fitted as eight Einstein modes. The lower-energy peaks correspond reasonably well with the known long-wavelength phonon branches [23] near 30, 45, and 80 cm^{-1}. On this scale, no anomalies are observed at either about 100 K or 40 K, demonstrating how subtle these transitions are.

Figure 10 shows an expansion at low temperatures with two different specific heat runs (taken upon heating the sample with a rate of 1 K min^{-1}) using the high-resolution heat flow technique. In one of the curves a jump appears at 28 K, indicating the presence of a second-order phase transition, which we ascribe to the lock-in transition of the incommensurate phase (expected near 40 K). We find that the occurrence of this transition depends strongly on the cooling history: in the first experiment the sample was cooled down slowly from room temperature over ∼4 h. The anomaly is present. We measured upon heating the sample over the transition up to ∼50 K, then cooled the sample down quickly (within 5 min) and repeated the experiment. The specific heat showed the same feature at 28 K. This time we heated the sample up to 150 K (over the temperature where we expected the transition to an incommensurate phase

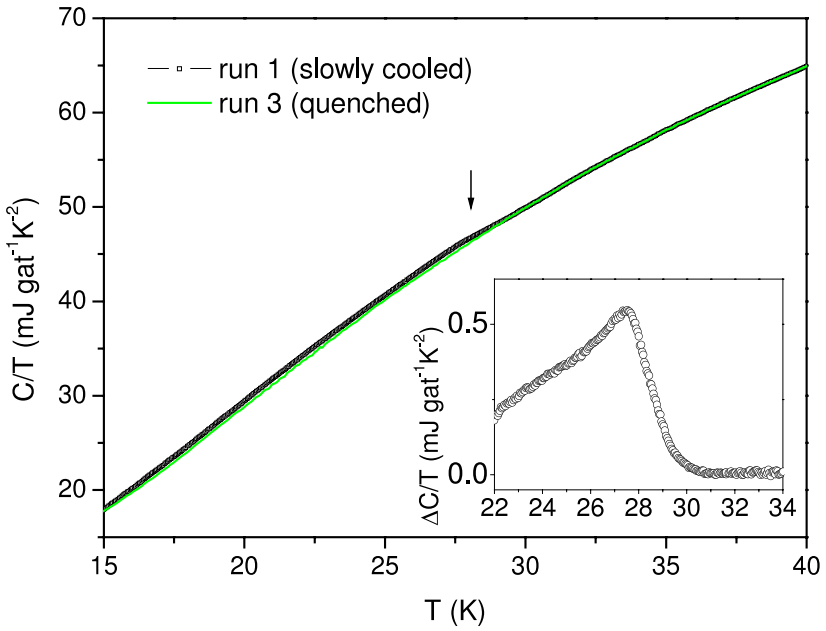

Figure 10. High-resolution specific heat data showing two runs with different cooling history: before run 1 the sample was slowly cooled down from room temperature over 4 h; before run 2 the sample was quenched down from 150 K within 10 min. The arrow marks a second-order phase transition in run 1. The inset of the figure shows the difference between run 1 and run 3.

at ∼110 K). Afterwards the sample was cooled down again more rapidly (within about 10 min) and a third run was performed. Surprisingly, the transition at 28 K is absent. The two curves included in figure 10 show the first run (after slow cooling from room temperature) and the third run after quenching the sample from 150 K. As the incommensurate transition is expected at ∼110 K, it seems that the occurrence of the 28 K transition depends on how fast the sample was cooled over the 110 K transition.

A more detailed examination of the phase transitions can be made by using the fit obtained from the set of eight Einstein modes to subtract the phonon background. Figure 11(a) shows the temperature range around 110 K and figure 11(b) shows the 28 K transition in detail. A broad anomaly in good accordance with the dielectric data is visible around 110 K, which we ascribe to the development of an incommensurate structure. The absence of a sharp feature suggests that the transition is more of a crossover and might be of glassy nature, which is reflected in its highly frequency dispersive dynamics. As the occurrence of the 28 K transition depends strongly on the cooling history, it seems that the system needs time to approach the incommensurate ground state. If the sample is quenched, the commensurate order persists down to low temperatures and the incommensurate lock-in transition is excluded.

If we look at the shape of the transition at 28 K, it appears rather like a slightly broadened mean field transition. However a slight upturn below the transition temperature might be attibuted to a critical behaviour, which is basically hidden by the broadening of the transition. We show, as a tentative comparison, a fit according to a power law of the form $C - C^{\text{phonon}} = A^{\pm}/\alpha|1 - T/T_c|^{-\alpha} + C^{\pm}$, with the critical exponent $\alpha = -0.166$, which corresponds to a 3D system with four components of the order parameter [24, 25] (as proposed by intrinsic theories); the critical amplitudes are $A^+ = A^- = 5.2$ mJ/gat K for $T > T_c$ and $T < T_c$, respectively, and $C^{\pm}$ is a constant. We do not attempt to perform a detailed analysis of the critical behaviour here,

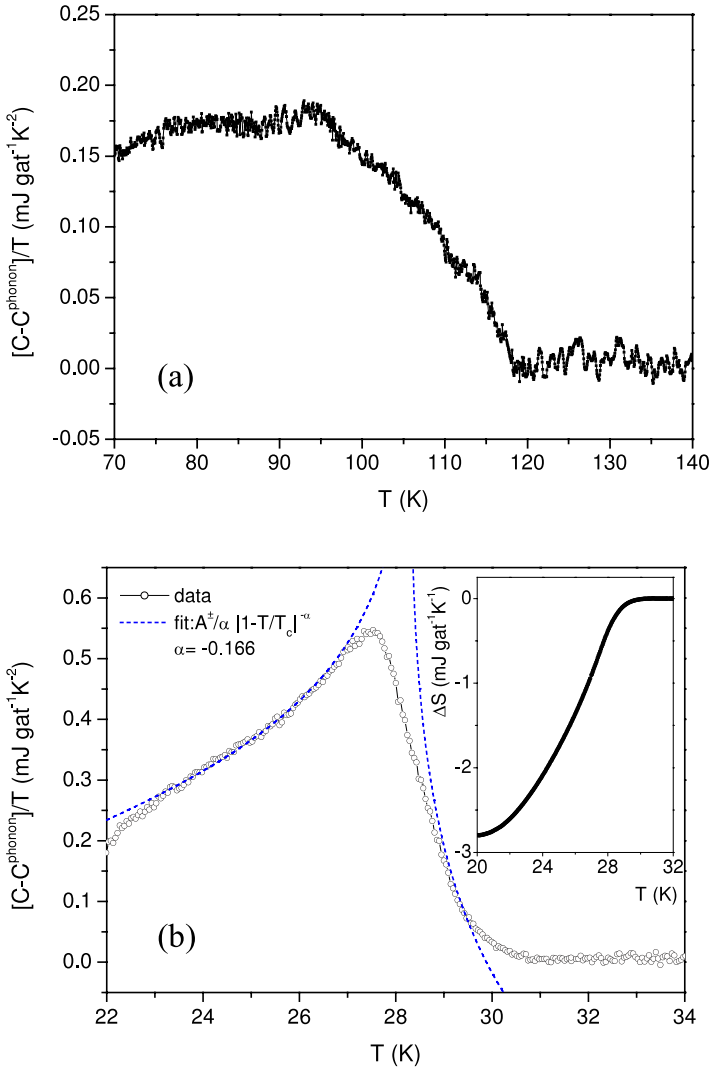

Figure 11. Specific heat after subtraction of the phonon background: (a) broad anomaly around 110 K, which we ascribe to the development of an incommensurate phase (adiabatic experiment); (b) second-order transition at 28 K, which might be the lock-in phase transition of the incommensurate phase (run1 heat-flow experiment). A fit according to a power law of the form $C - C^{\text{phonon}} = A^{\pm}/\alpha|1 - T/T_c|^{-\alpha} + C^{\pm}$ with the critical exponent $\alpha = -0.166$ has been added. Inset: entropy difference at the transition at 28 K, as obtained by integrating the specific heat data.

as the transition is too broad and we are not sure if the system is really in thermal equilibrium. Nevertheless, the fit with an exponent close to zero (logarithmic divergence) shows that large exponents such as $\alpha = 3/2$, which are expected from defect theory [26, 27], can be excluded as the divergence would be too strong. Both the incommensurate–commensurate transition at 103 K and that at about 582 K are expected to involve four-dimensional order parameters. The critical exponents for such systems are theoretically unusual, with polarization exponent $\beta = 0.39$, susceptibility exponent $\gamma = \gamma' = 1.385$, and specific heat exponent $\alpha = -0.166$. Note the very unusual sign of α; a negative exponent means that the divergence is slower than logarithmic (log is equivalent to an exponent of zero).

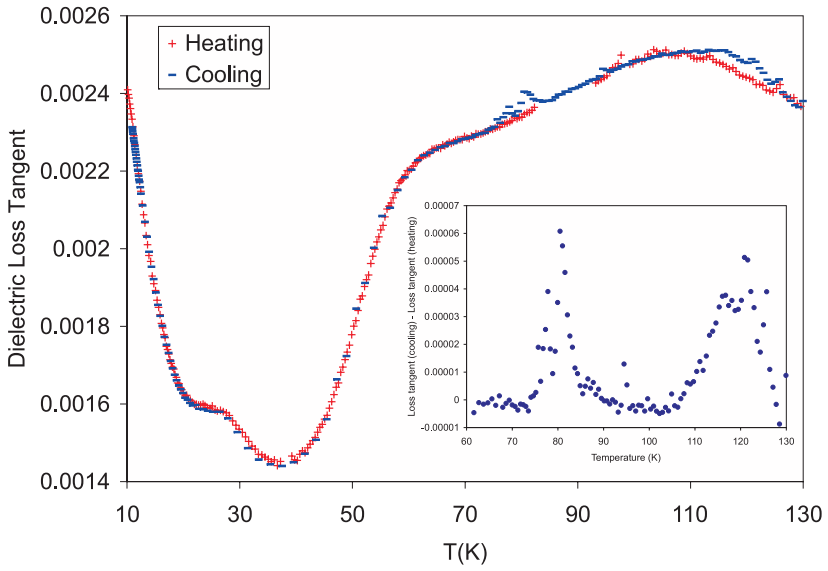

Figure 12. Dielectric loss tangent (10 kHz) measured upon slow dip cooling into liquid helium and subsequent re-heating. The inset shows the difference between the cooling and heating data between 60 and 130 K.

We note that, although the data are compatible with the theoretically predicted value of $\alpha = -0.166$ for four-dimensional order parameters, the uncertainty in this fitted value is large enough to include zero (in this case a logarithmic divergence is expected, which we found to be a less good fit than $\alpha = -0.166$), and a logarithmic divergence is compatible with mean field. Thus in the absence of an accurate value of gamma (precluded by the broad peak in susceptibility near 28 K), the present data do not in themselves provide evidence of 4D dynamics. The sluggish kinetics make us uncertain that the system is in true thermal equilibrium, which is an issue that has also been shown by Yakushkin [28] to arise in the specific heat data of the relaxor strontium barium niobate (SBN).

The inset in figure 11(b) shows the entropy difference at the transition at 28 K, as obtained from integrating the specific heat data. A total entropy change of 2.7 mJ/gat K is found. This rather small value is of interest in terms of the general discussion of lock-in transitions from incommensurate phases, which some authors have suggested are always first order.

3.3. Dielectric loss near 30 K

Following the realization that a slow cooling rate was an extremely important prerequisite for the observation of the transition near 30 K, we measured the dielectric response along the *b*-axis under slow dip cooling in liquid helium. In contrast to figure 1, we plot data here in terms of the dielectric loss tangent ($\varepsilon''/\varepsilon'$) to highlight two additional features of note (figure 12). A small feature is visible in the 20–30 K region, exactly where the anomaly in the specific heat was found (upon re-examination, the data in figure 1 also show this anomaly when plotted as dielectric loss). Additionally, a small hysteresis upon cooling and heating is observed in the region 110–125 K.

3.4. Entropy stabilization of incommensurate insulators

It is important to emphasize a qualitative difference between incommensurate structures in metals (or magnets) and in ferroelectric insulators: in metals or magnets the incommensurate

phase can be the $T = 0$ thermodynamic ground state. One calculates the internal energy U from the band structure and the Fermi level and finds, generically, that U can be minimal for a modulated incommensurate structure. In this sense, most incommensurate metals are more or less alike. However, incommensurate insulators are each different and idiosyncratic (although the axial next-nearest neighbour Ising model (ANNNI) gives a good overall description of many, especially the potassium selenate K_2SeO_4 family) and, most importantly, they are entropy stabilized: $G = U - TS$. Thus there are few, if any, insulators that are intrinsically incommensurate at $T = 0$ (a few may be defect-stabilized with defects pinning anti-phase boundaries). Therefore it should not be a surprise that the model of Cano and Levanyuk [5] does not apply to $Ba_2NaNb_5O_{15}$.

4. Conclusions

The present study serves as an update on the fine review of incommensurate phases in this material given by Schneck, Toledano and Errandonea [15] and studied 30 years ago throughout the 1970s and 1980s in a long series of papers by these well-known physicists. (It is interesting to note that Schneck is now a prominent concert pianist and Toledano is an opera singer.) Together with work recently reported [1] on the four phase transitions at high temperatures, there is now a relatively complete picture of seven phases and six transitions in this tungsten bronze.

References

[1] Scott J F, Hayward S A and Miyake M 2005 *J. Phys.: Condens. Matter* **17** 5911
[2] Buixaderas E, Kamba S and Petzelt P 2004 *Ferroelectrics* **308** 131
[3] Mori S, Yamamoto N, Koyama Y and Uesu Y 1997 *Phys. Rev.* B **55** 11212
[4] Fujishiro K and Uesu Y 1996 *J. Phys.: Condens. Matter* **8** 6435
[5] Cano A and Levanyuk A P 2004 *Phys. Rev. Lett.* **93** 245902
[6] Schneck J 1982 *PhD Thesis* Univ. Paris VI
[7] Scott J F, Shawabkeh A, Oliver W F, Larson A C and Vergamini P 1990 *Ferroelectrics* **104** 85
[8] Schneck J, Primot D, Von der Muhll R and Raves J 1977 *Solid State Commun.* **21** 57
[9] Verweft M, Van Tendeloo G, Van Landuyt J and Amelinckx S 1988 *Ferroelectrics* **88** 27
[10] Verweft M, Broddin D, Van Tendeloo G, Van Landuyt J and Amelinckx S 1989 *Phase Transit.* **14** 285
[11] Schneck J and Paquet D 1978 *Ferroelectrics* **21** 577
[12] Schneck J, Joukoff B and Mellet R 1980 *Ferroelectrics* **26** 775
[13] Oliver W F and Scott J F 1991 *Ferroelectrics* **117** 63
[14] Munteau L and Ailion D C 2000 *Phys. Rev.* B **63** 012406
[15] Toledano J C, Schneck J and Errandonea G 1986 *Incomensurate Phases in Dielectrics* ed R Blinc and A P Levanyuk (Amsterdam: Elsevier Science) pp 233–51
[16] Kutnjak Z, Filipič C, Levstik A and Pirc R 1993 *Phys. Rev. Lett.* **70** 4015
[17] Kutnjak Z, Pirc R, Levstik A, Levstik I, Filipič C, Blinc R and Kind R 1994 *Phys. Rev.* B **50** 12421
[18] Hemberger J, Böhmer R and Loidl A 1999 *Phase Transit.* **65** 231
[19] Fally M, Kubinec P, Fuith A, Warhanek H and Filipic C 1995 *J. Phys.: Condens. Matter* **7** 195
[20] Kubinec P, Fally M, Fuith A, Kabelka H and Filipic C 1995 *J. Phys.: Condens. Matter* **7** 2205
[21] Baski A A, Oliver W F and Scott J F 1987 *Ferroelectr. Lett.* **7** 171
[22] Ko J-H, Kojima S, Lushnikov S G, Katiyar R S, Kim T-H and Ro J-H 2002 *J. Appl. Phys.* **92** 1536
[23] Shawabkeh A and Scott J F 1991 *Phys. Rev.* B **43** 10999
[24] Mukamel D and Krinsky S 1976 *Phys. Rev.* B **13** 5078
[25] Toledano J C, Michel L, Toledano P and Brezin E 1985 *Phys. Rev.* B **31** 7171
Toledano J C and Toledano P 1987 *Landau Theory of Phase Transitions* (Singapore: World Scientific) p 448
[26] Imry Y and Wortis M 1979 *Phys. Rev.* B **19** 3580
[27] Levanyuk A P and Sigov A S 1979 *Izv. Akad. Nauk SSSR ser. Fiz.* **43** 1562
Levanyuk A P and Sigov A S 1988 *Defects and Structural Phase Transitions* (London: Gordon and Breach)
[28] Yakushkin E D 2004 *Fiz. Tverd. Tela* **46** 325